I. RESPONSE TO THE REVIEWERS

Comments to the EIC and the associate EIC:

We would sincerely like to thank you for conducting the review process for our manuscript and compiling all the reviews. In this revised version we have tried to address the remaining issues.We have also edited portions of the manuscript to improve the grammar and readability as suggested. The changes are also highlighted in the text.

Detailed response:

We thank all of you for taking your time and providing us with valuable, constructive suggestions. Your feedback really helped us improve the intellectual merit of this work.

Comments from Reviewer 1:

- *I vote to accept the present version, despite my reservation. I compliment the authors for the voluminous work that they have performed. Substantial effort has gone into this paper.*

  Our Response: We thank the reviewer for recognizing our effort. We believe that your comments have made this paper significantly better and help hone our understanding of the technical issues from a different point of view. This paper crosses the boundry between quantum mechanics and circuit theory, hence, there is a possibility of misunderstanding with regard to terminology that needed to be cleared up. In particular there is still a lingering misunderstanding.

  Errors are included in the expressions for power. The steady state polarization expression in Eq. 17, which is dependent on temperature, captures the kind of thermal errors that the reviewer is talking about. The error is plotted in Fig 5. It is possible to study the variation of error vs. power, by keeping temperature fixed, by varying kink energy and we will see the kind of relationship that the reviewer is referring to. Given the space limitation of this paper, we find it hard to consider all such relationships between error and power in a single paper.

Comments from Reviewer 2:

- *The paper addresses most of my concerns. Thank you for the revision.*

  Our Response: We sincerely thank the reviewer for taking time and providing us with his/her valuable feedback and suggestions.

Comments from Reviewer 3:

- *End of 1st paragraph of Sec. VI: "For large circuits the absolute values of the polarizations tend to deviate more from 1 hence the bounds will not be as tight for small circuits." Can you expand on why these polarizations drift more for large circuits since the clock signals should provide gain to the cells to boost their polarizations*

closer to 1/-1. Is this now covered on p. 21?

Our Response: We thank the reviewer for pointing this out. We think we did not make a clearer statement. The deviation in polarization depends on the size of each clock zone. For circuits, with larger clock zones, the absolute values of polarization tends to deviate more from 1/-1 due to increased possibilities of excited states. For such cases, our estimates will still hold, although they will not be as tight. So, using smaller clock zone will keep the polarization near 1/-1, and the actual extimates will be closer to our estimates, but still below it.

- *Is your notation in Eq. 34 as you desire?*

  Our Response: We thank the reviewer for pointing this out. We have changed it to *n* maximum values. The notation *k* is used in summation.

- *For the results of Fig. 5 and the text in the final paragraph of Sec. VII(A), readability may be improved by adding a Fig. 5(b) that shows either proportional scales or normalizes the y-axes of Fig. 5 in some way to show the significance of the difference in the change of both Energy and Polarization Error.*

  Our Response: We thank the reviewer for the suggestion. We have retracted our statement about proportionality of error change with power. It does not make sense to compare absolute values of different types of quantities. We now just state that they are inversely related.

- *Two separate comments on Table II.*

  Does the inverter figure show all cells used in the inverter? Most inverter designs would assume a cell at location (5,2), but you don't appear to have one. (Assume the input cell to be at location (1,2) and the darkest cell at location (3,2)).

  Our Response: The inverter design does have the cell at location (5,2), perhaps it did not show up in the print as it is colored yellow.

- *For the crossbar structure, the cell closest to the vertical input appears much darker (relatively) than any of the other cells close to the inputs of their respective circuits. Why is this occurring?*

  Our Response: This could be due to the rotated nature of the cells and specific nature of the circuit (depending on clock zones, type of cells and numbering of neighboring cells etc.). We do not think that there is any generalized observation here.

- *End of conclusion: "The power tool proposed in this work..." I would discourage the use of the word "tool" since you have a clear method in this paper, but no specific tool has been proposed.*

  Our Response: Changed.

- *The title states "Fast Estimation" and in other locations you talk about quickly estimating power, but give no*

indication in the paper of how fast your method is. Also, how does the computational time change as more
cells are added to the design? Your method implies a roughly linear increase in computational time, but some
evidence of speeding up the computation would be helpful.

Our Response: We thank the reviewer for suggesting this. The alternative method for estimating power is through coherence vector simulation, which will result in better estimates, but it is time consuming. We just need the estimates of the states, before and after an input change. These states can be estimated using a varity of fast methods. We used the probablistic method in [1], which is more than two orders of magnitude faster than coherence vector approach. We have now included this information in the Conclusion section.

Yes our method scales linearly with the number of cells, but is also dependent on the size of neighborhood considered in the computation of kink energy.

- *You introduce clocking zones in the Sec. I, but do not discuss clocking zones elsewhere in the paper. For many of the circuits presented in this work, would cells in different locations are likely to see different clocking energies (some dependence on distance from a clocking wire) and, especially for larger circuits, multiple clocking zones will be required. While an in depth discussion is probably not appropriate for this paper, some attention should be given to how power and concepts like thermal hotspots are influenced by these clocking issues. Also, how are you "clocking" your examples in Sec. VII?*

Our Response: Our estimates are upper bounds of power estimates and are independent of the actual clocking zone structure. The bounds will hold under variation of clocking zones. However, the reviewer is right in pointing this out that we do not consider the variation of clocking energy within the zones. We now mention this in Section VI.

- *Also, please review your paper for grammar/readability. There are numerous small sections that upon being fixed would greatly improve the readability of this paper (i.e. the second sentence of the caption of Table II..) Overall, this paper probably needs to be reorganized and repackaged a bit...*

Our Response: We have changed the caption as suggested by the reviewer. We have re-read our paper and fixed grammar as best as we can.

- *One thing that Reviewer 3 points out is that worrying about hotspots at this point and time is probably a bit premature. That's not to say that your estimator doesn't have merit – but you should use it to show for perhaps a specific circuit that it performs X times better than previous methods for power estimation. Then, perhaps based on those power results, make a case for why we should be looking at QCA – perhaps via some comparison to a CMOS circuit, etc.*

Our Response: We agree with the reviewer that such a study will surely help to promote QCA as a promising future technology. The only other alternative is the coherence vector formalism of Timler. Our theory shows exactly how our estimate is related to it in terms of accuracy. Ours is an upper bound. We have now included

the speed up information that our estimating strategy offers in the Conclusion section.

Estimation of Upper Bound of Power Dissipation in QCA Circuits

Saket Srivastava*, Sudeep Sarkar† and Sanjukta Bhanja*

* Electrical Engineering,† Computer Science and Engineering

University of South Florida, Tampa, Florida.

Emails: ssrivast@mail.usf.edu, bhanja@eng.usf.edu, sarkar@cse.usf.edu

Abstract

Quantum-dot cellular automata (QCA) is a field-coupled computing paradigm. States of a cell change due to mutual interactions of either electrostatic or magnetic fields. Due to their small sizes, power is an important design parameter. In this work, we derive an upper bound for power loss that will occur with input change, even with the circuit staying at respective ground states before and after the change. This bound is computationally efficient to compute for large QCA circuits since it just requires the knowledge of the before and after ground states due to input change. We categorize power loss in clocked QCA circuits into two types that are commonly used in circuit theory: switching power and leakage power. Leakage power loss is independent of input states and occurs when the clock energy is raised or lowered to depolarize or polarize a cell. Switching power is dependent on input combinations and occurs at the instant when the cell actually changes state. Total power loss is controlled by changing the rate of change of transitions in the clocking function. Our model provides an estimate of power loss in a QCA circuit for clocks with sharp transitions, which result in non-adiabatic operations and gives us the upper bound of power expended. We derive expressions for upper bounds of switching and leakage power that are easy to compute. Upper bounds obviously are pessimistic estimates, but are necessary to design robust circuits, leaving room for operational manufacturing variability. Given that thermal issues are critical to QCA designs, we show how our model can be valuable for QCA design automation in multiple ways. It can be used to quickly locate potential thermal hot spots in a QCA circuit. The model can also be used to correlate power loss with different input vector switching; power loss is dependent on the input vector. We can study the trade-off between switching and leakage power in QCA circuits. And, we can use the model to vet different designs of the same logic, which we demonstrate for the full adder.

II. INTRODUCTION

In Quantum-dot Cellular Automata (QCA) architecture, computation is performed by relying on device to device interactions. Elementary units are the QCA cells that typically contain two electrons and four possible dot location at each corner of a QCA cell. There are two ground states for each cell, which can be used to represent 0 or 1. The state of a cell is determined by the Coulombic interactions with neighboring cell states. The intended logic is mapped to the ground state of the configuration. While there is no or very little quantum entanglement between cells, there is significant entanglement between the dots within a cell. The extent of the entanglement is determined

by the tunneling energy, which is used to depolarize a cell (nullify the cell state) or to latch it to a 0 or 1 state. Current proposals for QCA designs rely on a set of 4 clocks, phase shifted with respect to each other, and used to "push" information from inputs to the output by modifying the cell tunneling energy. The complete circuit is divided into zones, each associated with one of the 4 clocks in sequence. Each clock lags by 90 degrees in phase with respect to the previous clocking signal. A cell latches to the next states, based on the neighboring cells, when the clock is low, and is depolarized when the clock is high. This induces a wave like flow of information across circuit.

QCA is an emerging technology that is unfolding at a consistent pace. Both individual QCA cell (semi-conductor and metallic) and multiple QCA arrangement, such as wire and majority logic, have been fabricated and tested [2]. More recently, lot of work is being put into fabricating molecular QCA [3], [4], [5] and magnetic QCA [6], [7]. Both magnetic and molecular QCA will make room temperature operation possible, which currently appears to be the major bottleneck in transitioning this exciting nanotechnology into practice.

Unlike computation mechanisms that involve the transfer or flow of electrons, such as CMOS gates, QCA computation does not involve electron transfer between adjacent QCA cells. Since only few electrons are involved in QCA computations, it is susceptible to thermal issues. Therefore it is important to model and to consider power as an important parameter during the QCA design process at multiple levels of design abstraction along with errors [8], [9], [10] and defects [11], [12].

While work on defect and faults in QCA circuits, which are other important issues, have started [11], [9], [13], power issues have not been considered extensively. Perhaps the most pure power model is the quantum-mechanical model of the temporal dynamics of power derived by Timler and Lent [14], [15]. They identified three components of power: clock power, cell to cell power gain, and power dissipation. While this model gives us physically close estimates, it is computationally expensive to estimate. When designing QCA circuits, we would like estimate power quickly in order to choose among many different alternatives and parameters. The need for full blown quantum-mechanical estimation will be relegated to the very end of the design process. To this end, some studies [16], [17] present lower bounds of power dissipated that are easy to compute. However, from a design automation point of view it is important to design for the worst case, leaving us with margin for errors due to process variability. *Here worst case refers to the power dissipated during a non-adiabatic clocking scheme*. For worst case considerations, the upper bound for power is more relevant. We derive such an upper bound and show how it can be relevant for QCA design automation. Some other relevant power related works include the energy vs. speed trade-off study in [18] for different clocking schemes, however, in the context of reversible computing. In [19], an RC model for a clocked QCA chain is used to investigate power dissipation under adiabatic clocking scheme.

Under the Hartree-Fock quantum mechanical approximation, which has been found to be adequate, the dynamics of a collection of QCA cells can be expressed in terms of the dynamics of individual cells. As a result, the power dissipation for a QCA circuit can be expressed as the sum of power estimates computed on a per-cell basis. Each cell in a QCA circuit sees three types of events: (i) clock going from low to high so as to "depolarize" a cell, (ii) input or cells in previous clock zone switching states, and (iii) clock changing from high to low, latching and

holding the cell state to the new state. Each of these events are associated with power loss. An interesting point is that the power dissipated during the first and the third transitions is due to the clock changing and occurs even if the state of a cell does not change. This is analogous to "leakage" power in CMOS circuits. The power loss due to the second event can be termed as the "switching" power since it is dependent on the cells actually changing states. Clock energy needs to be high to drive the cell into an intermediate, depolarized state. In a fully depolarized state, the change in driver polarization has no effect on the driven cell, hence the "switching" power is zero. This is the ideal case. However, to achieve this the clocking energy needs to be high and, consequently, the associated "leakage" power would be high. Thus, these two components of power are inversely related. The upper bounds derived in this paper will help us quantify this relationship. However, a real clock implementation will also add to power loss in the clocking circuit itself. This will add to the overall power dissipation in a QCA circuit. In this study we do not account for such power loss.

Adiabaticity of a system depends on the rate of exchange of energy between the system and the environment. In QCA, a clock is used as a means to lower and raise energy barriers and to provide power to the system. Hence adiabaticity of a QCA circuit operation can be controlled by controlling the rate of change of clock. Higher clock smoothing slows changes of state and hence increases degree of adiabaticity. To arrive at the upper bound of the power loss, we consider the limiting case of instantaneous change by modeling these events as step functions. In this work when we mention *non-adiabatic power dissipation* in a QCA circuit, we refer to power dissipation with step changes. We presented an early and shortened version of this bound derivation in [20], however, using very small QCA logic elements. The theoretical contributions of this work are (i) the computation of upper bound of power dissipated in a QCA cell representing the worst case input switching vector set and (ii) the characterization of power into two components: leakage and switching. This upper bound, which is easy to compute, can be used in the QCA circuit design process. Further, we demonstrate how these estimates can be used (iii) to characterize the power dissipation in basic QCA elements like the inverter, majority gate, and crossbar, (iv) to compare two functionally equivalent adder circuits in terms of power dissipated during any switching event, (v) to compute power in large QCA circuit like a 4x1 Multiplexer and a single bit ALU, (vi) to study variation of power expended with different input states, and (vii) to locate the thermal weak spots in a design.

The organization of this paper is as follows. We first present the quantum modeling of a single QCA cell in Section III. Section IV summarizes the quantum formulation of the power dissipation in QCAs derived from the basic principles to arrive at a model presented in [14]. Using this expression, we derive the upper bound for the power dissipated in a QCA cell during each clock cycle in Section V. We then use this per cell bound to estimate the power in the whole circuit as described in Section VI. Finally, in Section VII we show simulation results using this upper bound. We first validate the bound using quantum mechanical simulations. We then demonstrate the power estimation process and study energy dissipation of logic elements such as majority gates, inverter, single bit adders and also for large QCA circuits such as a 4x1 multiplexer and a single bit ALU [21].

III. HAMILTONIAN OF QCA CELL

We first review the quantum modeling of a QCA cell collection, without considering the environment. Each QCA cell, be it one electron in two dots, as in molecular-QCA, or a cell with two electrons with four dots, is constructed to have two ground states $|0\rangle$ and $|1\rangle$. An array of cells can be modeled fairly well by considering cell-level quantum entanglement of these two states and just Coulombic interactions with nearby cells, using the Hartee-Fock (HF) approximation [22], [23]. This allows one to characterize the evolution of the individual wave functions. The state of a cell at time t, $|\Psi(t)\rangle$, is a linear combination of these two states, i.e. $|\Psi(t)\rangle = c_0(t)|0\rangle + c_1(t)|1\rangle$. The coefficients, $c_0(t)$ and $c_1(t)$, are functions of time. The expected value of any observable, $\langle \hat{A}(t)\rangle$, can be expressed in terms of the wave function as $\langle \hat{A}\rangle = \langle \Psi(t)|\hat{A}(t)|\Psi(t)\rangle$ or equivalently as $\text{Tr}[\hat{A}(t)|\Psi(t)\rangle\langle\Psi(t)|]$, where Tr denotes the trace operation, $\text{Tr}[\cdots] = \langle 0|\cdots|0\rangle + \langle 1|\cdots|1\rangle$. The term $|\Psi(t)\rangle\langle\Psi(t)|$ is known as the density operator, $\hat{\rho}(t)$. Expected value of any observable of a quantum system can be computed if $\hat{\rho}(t)$ is known.

The entries of the density matrix, $\hat{\rho}_{ij}(t)$, is defined by $c_i(t)c_j^\dagger(t)$ or $\hat{\rho}(t) = \mathbf{c}(t)\mathbf{c}(t)^\dagger$, where † denotes the conjugate transpose operation. Note that the density matrix is Hermitian, i.e. $\hat{\rho}(t) = \hat{\rho}(t)^\dagger$. Each diagonal term, $\hat{\rho}_{ii}(t) = |c_i(t)|^2$, represents the *probability* of finding the system in state $|i\rangle$. It can be easily shown that $\hat{\rho}_{00}(t) + \hat{\rho}_{11}(t) = 1$. In QCA device modeling literature, one uses the concept of *polarization*, x, to characterize the state of a cell and is simply $\hat{\rho}_{11}(t) - \hat{\rho}_{00}(t)$, the difference of the two probabilities. It ranges from -1 to 1.

The density operator is a function of time, $\hat{\rho}(t)$, and its dynamics is captured by the Loiuville equation or the von Neumann equation, which can derived from the basic Schrodinger equations that capture the evolution of the wave function over time, $\Psi(t)$.

$$\hbar\frac{\partial}{\partial t}\hat{\rho}(t) \quad = \quad \hat{H}_S\hat{\rho}(t) - \hat{\rho}(t)\hat{H}_S \tag{1}$$

where $\hat{H}_S$ is a 2 by 2 matrix representing the Hamiltonian of the cell. For arrangements of QCA cells, it is common to assume only Coulombic interactions between cells and use the Hartree-Fock approximation to arrive at the matrix representation of the Hamiltonian given by [22]

$$\hat{H}_S = \begin{bmatrix} -\frac{1}{2}\sum_i E_k x_i f_i & -\gamma \\ -\gamma & \frac{1}{2}\sum_i E_k x_i f_i \end{bmatrix} = \begin{bmatrix} -\frac{1}{2}G & -\gamma \\ -\gamma & \frac{1}{2}G \end{bmatrix} \tag{2}$$

where the sums are over the cells. E_k is the energy cost of two neighboring cells with opposite polarizations; this is also referred to as the "kink energy". f_i is the geometric factor capturing electrostatic fall off with distance between cells. x_i is the polarization of the i-th neighboring cell. The tunneling energy between the two states of a cell, which is controlled by the clocking mechanism, is denoted by γ. For notational simplification, we will use G to denote the total kink energy due to the polarized neighbors.

IV. QUANTUM MECHANICAL POWER

In most cases, power dissipation can be linked to the interaction of the quantum system with its environment (reservoir or bath), i.e. we have open quantum systems. There are a number of different methods to analyze such dissipative quantum systems [24], [25] and is an open research area. Each approach involves making different

assumptions. The most physically based approaches are those that model the interaction of the system with its environment and treat the system plus environment as one closed system. Let S be the quantum system under consideration, which in our case is the QCA cell and let E denote the external bath. The state vector of the closed system $S+E$ is $|\Psi\rangle$ and the corresponding density matrix is $\hat{\rho}_{S+E} = |\Psi\rangle\langle\Psi|$. To derive the density matrix, $\hat{\rho}$, of the subsystem S, we will have to average (or marginalize, adopting terminology from probability theory) over the environment, i.e. by taking a trace over E.

$$\hat{\rho} = \text{Tr}_E \hat{\rho}_{S+E} \tag{3}$$

This is the reduced density matrix of the system S. It is different from the density matrix of system S alone as it includes the effect of E. The average of any observable of interest of this system, such as the Hamiltonian (or energy), can be expressed in terms of this reduced density matrix.

$$|\Psi\rangle \hat{H} \langle\Psi| = \langle \hat{H} \rangle_{\hat{\rho}} = \text{Tr}\{\hat{H}_S \hat{\rho}\} \tag{4}$$

There are many approaches, each making its own assumptions, to deriving the equation governing the dynamics of the reduced density matrix from the Loiuville equation for $\hat{\rho}_{S+E}$. We will not go into details of these approaches here. However, we will adopt the theoretical arguments made by Lindblad regarding the constraint that should be satisfied by the dynamics of the density matrix of any open system [26], [23]. Lindblad reasoned from a purely mathematical point of view. The time evolution of the density operator is a unitary map. The possible transformations have to be "completely positive". That is, $\hat{\rho} \rightarrow \sum_n \hat{O}_n \hat{\rho} \hat{O}_n^\dagger$, where $\hat{O}_n$ is a set of linear operators on the reduced state space with $\sum_n \hat{O}_n^\dagger \hat{O}_n = 1$. This latter condition guarantees that $\text{Tr}\{\hat{\rho}\}$ does not change. The most general form of the time evolution of the reduced density matrix preserving its trace is the Lindblad form of the quantum master equation given by

$$\frac{\partial}{\partial t}\hat{\rho} = -\frac{i}{\hbar}[H_S, \hat{\rho}]_- + \frac{1}{2}\sum_{m,n=1}^{s^2-1} A_{mn}\left(2\hat{L}_m \hat{\rho} \hat{L}_n^\dagger - \hat{\rho}\hat{L}_n^\dagger \hat{L}_m - \hat{L}_n^\dagger \hat{L}_m \hat{\rho}\right) \tag{5}$$

where H_S is the Hamiltonian of just the quantum system, S, and $\hat{L}_m$ are the Lindblad operators capturing the damping effect of the environment. For a system with s states, there will be $s^2 - 1$ Lindblad operators. Thus, for a two-state system, such as our QCAs, we have $\{\hat{L}_1, \hat{L}_2, \hat{L}_3\}$. The Lindblad operators have zero trace, $\text{Tr}\{\hat{L}_m\} = 0$, and are orthonormal to each other, $\text{Tr}\{\hat{L}_m \hat{L}_n^\dagger\} = \delta_{mn}$. Along with the identity operator they form an orthogonal basis for the Lindblad space. The parameter matrix $\{A_{mn}\}$ is Hermitian and positive semidefinite. Sometimes for notational convenience, the term with Lindblad operators is represented as the Lindblad super-operator, $\mathcal{L}$.

$$\mathcal{L}(\hat{\rho}) = \frac{1}{2}\sum_{m,n=1}^{s^2-1} A_{mn}\left(2\hat{L}_m \hat{\rho} \hat{L}_n^\dagger - \hat{\rho}\hat{L}_n^\dagger \hat{L}_m - \hat{L}_n^\dagger \hat{L}_m \hat{\rho}\right) \tag{6}$$

Notice that without the Lindblad super-operator, the evolution equation is the standard Loiuville equation for an isolated system. The Lindblad form of the evolution of density matrix can be related to efforts in capturing dissipation using non-Hermitian Hamiltonian terms (see [23]), however, charges are not preserved in such models.

Although the Lindblad equation seems to be the most general form for the dynamics of open systems, the underlying complete positivity assumption is valid under certain conditions [24]: (i) weak coupling between S and

E, so that the initial density matrix can be factored as $\hat{\rho}_{S+E} = \hat{\rho} \otimes \hat{\rho}_E$, (ii) Markov approximation, i.e. the reduced density operators change more slowly than the time-range of correlations within the environment, and (iii) the temperature is not too low. Even with these assumptions, this type of modeling of the dissipation has been found to be useful for many quantum situations, such as in NMR [24].

A. Damped Bloch Equation for QCA cell

The Lindblad operators, $\hat{L}_m$, describes the effort of the environment in the Markov approximation. The form of the Lindblad operators specifies the nature of the dissipative process. For a 2-state system, like our QCA cell, these can be chosen to be the normalized Pauli matrices.

$$\hat{L}_1 = \tfrac{1}{\sqrt{2}}\hat{\sigma}_1 = \tfrac{1}{\sqrt{2}}\begin{bmatrix} 0 & 1 \\ 1 & 0 \end{bmatrix}, \quad \hat{L}_2 = \tfrac{1}{\sqrt{2}}\hat{\sigma}_2 = \tfrac{1}{\sqrt{2}}\begin{bmatrix} 0 & i \\ -i & 0 \end{bmatrix}, \quad \hat{L}_3 = \tfrac{1}{\sqrt{2}}\hat{\sigma}_3 = \tfrac{1}{\sqrt{2}}\begin{bmatrix} -1 & 0 \\ 0 & 1 \end{bmatrix} \tag{7}$$

The operator $\hat{L}_1$ represents a bit flip error, $\hat{L}_3$ represents a dephasing error, and $\hat{L}_2$ represents a combination of bit flip and dephasing error. These three error "channels" are coupled through the parameter matrix, $\{A_{mn}\}$. Thus, for the two-state case, the Lindblad super-operator can be written as

$$\mathcal{L}(\hat{\rho}) = \frac{1}{2} \sum_{m,n=1}^{3} A_{mn} \left(2\hat{\sigma}_m \hat{\rho} \hat{\sigma}_n^\dagger - \hat{\rho}\hat{\sigma}_n^\dagger \hat{\sigma}_m - \hat{\sigma}_n^\dagger \hat{\sigma}_m \hat{\rho} \right) \tag{8}$$

The Lindblad equation (Eq. 5) can be further simplified by expressing the evolution of the density matrix in the operator space. We know that the 2 by 2 density matrix can be expressed as a combination of the Pauli operators.

$$\hat{\rho} = \frac{1}{2}\hat{I} + \frac{1}{2}\sum_{k=1}^{3} \lambda_k \hat{\sigma}_k \tag{9}$$

The resulting coefficients form the coherence vector representation of the density matrix, $\vec{\lambda} = \begin{bmatrix} \lambda_1, & \lambda_2, & \lambda_3 \end{bmatrix}^T$. Using Eq. 9 in Eq. 8 and taking the trace with each of Pauli matrices, we arrive at the damped Bloch equation given by:

$$\frac{d}{dt}\vec{\lambda} = \vec{\Gamma}_S \times \vec{\lambda} + \xi\vec{\lambda} + \vec{\eta} \tag{10}$$

where $\vec{\Gamma}_S$ is a real three-dimensional energy vector obtained by projecting the two state Hamiltonian for a QCA cell onto the basis of generators.

$$\Gamma_S = \frac{Tr\{\hat{H}\hat{\sigma}\}}{\hbar} = \frac{1}{\hbar}\begin{bmatrix} -2\gamma, & 0, & G \end{bmatrix}. \tag{11}$$

The entries of the 3 by 3 damping matrix ξ is given by

$$\xi(i,j) = \frac{1}{2}\text{Tr}\{\mathcal{L}(\hat{\sigma}_i)\hat{\sigma}_j\} \tag{12}$$

and the entries of the constant vector are given by

$$\eta(i) = \frac{1}{2}\text{Tr}\{\mathcal{L}(\hat{I})\hat{\sigma}_j\} \tag{13}$$

Using the properties of the Pauli operators that $\hat{\sigma}_1\hat{\sigma}_2 = i\sigma_3, \hat{\sigma}_2\hat{\sigma}_3 = i\sigma_1, \hat{\sigma}_3\hat{\sigma}_1 = i\sigma_2$, and $\hat{\sigma}_1\hat{\sigma}_1 = \hat{\sigma}_2\hat{\sigma}_2 = \hat{\sigma}_3\hat{\sigma}_3 = \hat{1}$, we can show that the damping matrix is a diagonal matrix with entries given by

$$\xi(i,j) = \begin{cases} A_{ij} + A_{ji} & \text{for } i \neq j \\ -2\sum_{m \neq i} A_{mm} & \text{for } i = j \end{cases} \tag{14}$$

Note that the off-diagonal terms are real since the matrix A is Hermitian. The off diagonal terms would be zero if the channel interaction terms A_{ij} had a zero real component. The constant term is given by

$$\eta = 2i \begin{bmatrix} A_{23} - A_{32} \\ A_{13} - A_{31} \\ A_{12} - A_{21} \end{bmatrix} \tag{15}$$

Note that since the parameter matrix A is Hermitian, the vector η is real, governed by the imaginary values of the off diagonal terms of the A matrix, capturing the interaction between the different dissipation channels.

B. Choice of Environment Parameters

We will choose the off-diagonal terms, or rather the η terms, such that the dynamics represent inelastic dissipative heat bath coupling (open world), with the system moving towards the ground state [22], [23]. Thus, setting $\frac{d}{dt}\vec{\lambda}$ to zero, we have.

$$\vec{\eta} = -\vec{\Gamma}_S \times \vec{\lambda}^{ss} - \xi\vec{\lambda}^{ss} = \begin{bmatrix} 2(A_{22}+A_{33}) & -(A_{12}+A_{21})+G/\hbar & -(A_{13}+A_{31}) \\ -(A_{12}+A_{21})-G/\hbar & 2(A_{11}+A_{33}) & -(A_{23}+A_{32})-2\gamma/\hbar \\ -(A_{13}+A_{31}) & -(A_{23}+A_{32})+2\gamma/\hbar & 2(A_{11}+A_{33}) \end{bmatrix} \lambda^{ss} \tag{16}$$

The steady-state coherence vector, λ^{ss}, can be derived from the steady-state density matrix at thermal equilibrium.

$$\hat{\rho}^{ss} = \frac{e^{-\hat{H}_S/kT}}{\text{Tr}[e^{-\hat{H}_S/kT}]} \tag{17}$$

where k is the Boltzman constant and T is the temperature. The corresponding steady state coherence vector is given by

$$\vec{\lambda}^{ss} = \text{Tr}\{\hat{\rho}^{ss}\hat{\sigma}\} = -\frac{\vec{\Gamma}_S}{|\vec{\Gamma}_S|} \tanh\Delta = \frac{\tanh\Delta}{\Omega} \begin{bmatrix} -2\gamma \\ 0 \\ G \end{bmatrix} \tag{18}$$

where $\Delta = \frac{\Omega}{kT}$, is the thermal ratio, with $\Omega = \sqrt{4\gamma^2 + G^2}$, the energy term (also known as the Rabi frequency).

Upon matching the expression for λ^{ss} in Eq. 16 with the expression for η in Eq. 15, we see that the condition $A_{13} = A_{31} = 0$ must hold, i.e. there cannot be any interaction between the pure bit-flip and pure dephasing channels. This is not much of problem since a combination of bit-flip and dephasing is capture by the second channel. Without attaching importance to any particular channel, we assume that the diagonal parameters associated with each of the channels are the same, i.e. $A_{11} = A_{22} = A_{33} = \frac{1}{4\tau}$, where τ can be looked upon as a channel time constant. The factor of 4 is used to simplify expressions. We will also assume that the interactions between first and second

channels and between second and third channels, which can exist, is captured by purely imaginary values, i.e. real parts of A_{12}, A_{21}, A_{23}, and A_{32} are zero. With these assumptions, we have

$$\vec{\eta} = \frac{1}{\tau}\vec{\lambda}^{ss} \text{ and } \xi = - \begin{bmatrix} \frac{1}{\tau} & 0 & 0 \\ 0 & \frac{1}{\tau} & 0 \\ 0 & 0 & \frac{1}{\tau} \end{bmatrix} \tag{19}$$

Using these in Eq. 10 we have

$$\frac{d}{dt}\vec{\lambda} = \vec{\Gamma}_S \times \vec{\lambda} - \frac{1}{\tau}\left(\vec{\lambda} - \vec{\lambda}^{ss}\right) \tag{20}$$

where τ can be looked upon as the energy relaxation time. If $\tau \to \infty$, it represents the absence of any dissipation. Lower the value of τ, faster the heat dissipation away from the cell. This is essentially the expression that was used by Timler and Lent [14]. Here we have spelt out the underlying assumptions in this form.

C. Power Loss

The expected value of the Hamiltonian at each time instant is given by

$$E = \langle H \rangle = \frac{\hbar}{2}\vec{\Gamma} \cdot \vec{\lambda} \tag{21}$$

The equation for the instantaneous power is given by

$$P_{total} = \frac{d}{dt}E = \frac{\hbar}{2}\left(\frac{d}{dt}\vec{\Gamma}\right) \cdot \vec{\lambda} + \frac{\hbar}{2}\vec{\Gamma} \cdot \left(\frac{d}{dt}\vec{\lambda}\right) \tag{22}$$

The first term captures the power in and out of the clock and cell to cell power flow. The second term represents the dissipated power. It is this quantity that we are interested in.

$$P_{diss}(t) = \frac{\hbar}{2}\vec{\Gamma}(t) \cdot \left(\frac{d}{dt}\vec{\lambda}(t)\right) \tag{23}$$

V. UPPER BOUND FOR POWER DISSIPATION

Coupling the expression for power dissipation with the damped Bloch equation we see that

$$P_{diss}(t) = -\frac{\hbar}{2\tau}\vec{\Gamma}(t) \cdot \left(\vec{\lambda}(t) - \vec{\lambda}^{ss}(t)\right) \tag{24}$$

If the instantaneous coherence vector tracks the steady state coherence vector for that time instant, i.e. $\vec{\lambda}(t) \approx \vec{\lambda}^{ss}(t)$ then the power dissipated is very low (i.e. very close to the adiabatic limit). Fig. 1(a) depicts the condition when the driver polarization switches from -1 to 1. The top plot of Fig. 1(a) shows the change in the driver polarization and the associated change in the steady state polarization $\vec{\lambda}_3^{ss}(t)$. Note that in this case, the cell polarization $\vec{\lambda}_3(t)$ tracks the steady state value quite well. The bottom plot of Fig. 1(a) shows the clock energy change and the power dissipated. We note that there is only slight loss of power during the switching of the driver polarization. Fig. 1(b), is for the case of no change in driver polarization. Here the power dissipation is very low.

High dissipation situation arises when $\vec{\lambda}(t)$ lags the changing $\vec{\lambda}^{ss}(t)$, which will happen under non-adiabatic clocks. From Eq. 18 we can see that $\vec{\lambda}^{ss}$ changes whenever the underlying Hamiltonian changes, which happens when (i) clock goes from low to high ($\gamma_L \to \gamma_H$) so as to "depolarize" a cell, (ii) input or cells in previous clock
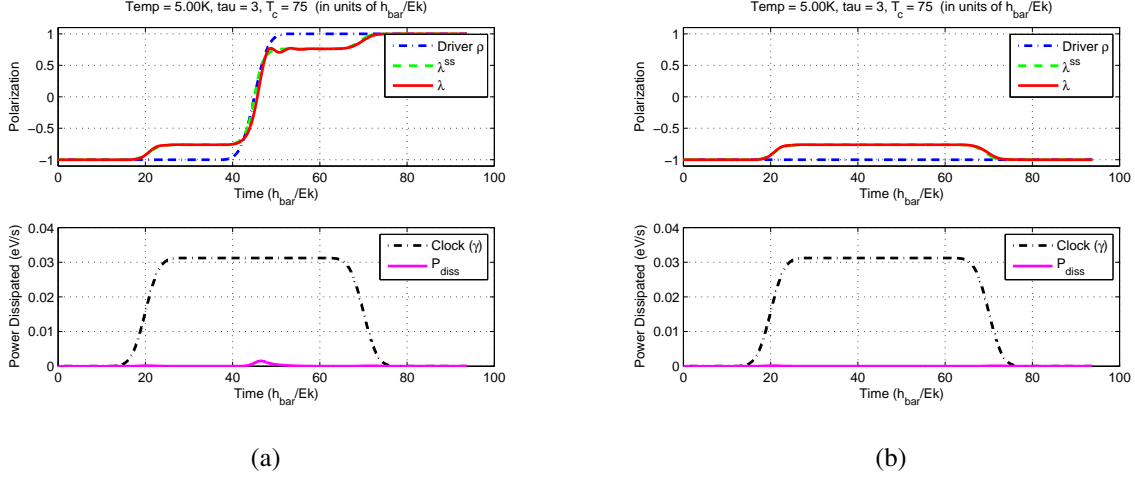
Fig. 1. (Color) Polarization change (top plot) and power loss (bottom plot) in a single cell when its polarization changes from (a) -1 to 1 (or 0 to 1 logic) and (b) -1 to -1 (remains at state 0) during a quasi-adiabatic clocking scheme.
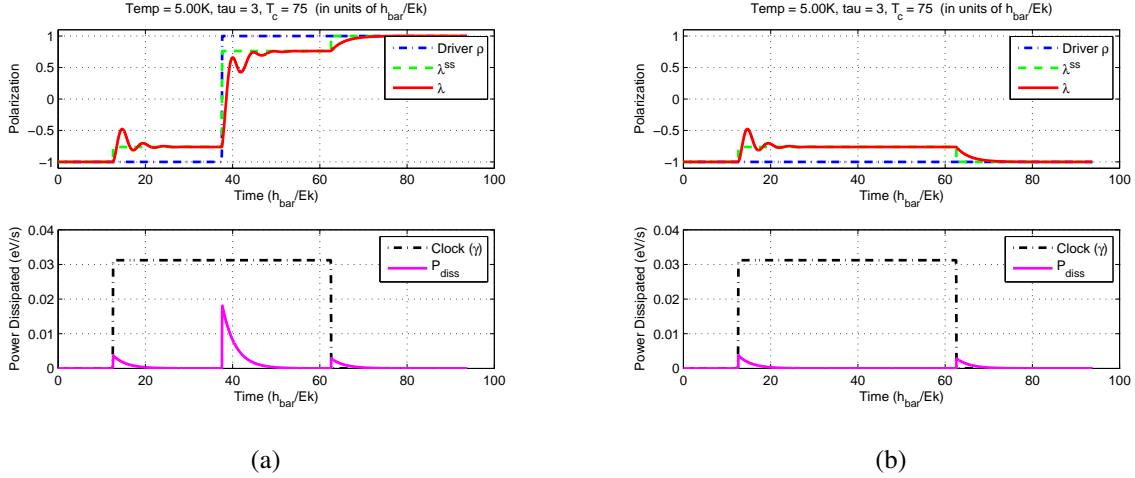

Fig. 2. (Color) Polarization change (top plot) and power loss (bottom plot) in a single cell when its polarization changes from (a) -1 to 1 (or 0 to 1 logic) and (b) -1 to -1 (no change in state) during non-adiabatic clocking scheme

zone switches states ($G_- \rightarrow G_+$), and (iii) clock changes from high to low ($\gamma_H \rightarrow \gamma_L$), latching and holding the cell state to the new state. Fig. 2(a) shows the switching behavior and power dissipation for abrupt change in driver polarization and clocking. As we can see from the graph, the steady state polarization $\vec{\lambda}_3(t)$ of the cell is not able to follow the corresponding steady state polarization. There is some lag and ripple associated with the change. This leads to power loss, which is shown in the bottom plot of Fig. 2(a). Note that there is power loss for all the three events. Fig. 2(b) shows the same switching behavior and power dissipation in the cell during a non adiabatic event even when the driver polarization remains the same (-1 to -1 switching). As we can see from the graphs, the total power dissipated by the cell occurs not only when its polarization changes, but a significant amount of power loss

also occurs when the clock energy barriers are raised and lowered. The faster the changes involved in these events, the more the power dissipation. To arrive at the upper bound of the power loss, we consider the limiting case of instantaneous change; we model these events using as step functions.

We derive the energy dissipated for each of these three events by integrating around them. Without loss of generality, let the event under consideration be centered at $t = 0$. We integrate over $[-D, D]$, such that $D \gg \tau$, i.e. the integration time period is much larger than the relaxation time constant. This, of course, places limit on the clock speed. This constraint is natural also for correct operation; clock period should be larger than the relaxation time constants otherwise errors will arise. Energy dissipated over a time period $[-D, D]$ can be arrived at by integrating $P_{diss}(t)$.

$$
\begin{aligned}
E_{diss} &= \frac{\hbar}{2} \int_{-D}^{D} \vec{\Gamma} \cdot \frac{d\vec{\lambda}}{dt} dt \\
&= \frac{\hbar}{2} \left(\left[\vec{\Gamma} \cdot \vec{\lambda} \right]_{-D}^{D} - \int_{-D}^{D} \vec{\lambda} \cdot \frac{d\vec{\Gamma}}{dt} dt \right) \\
&= \frac{\hbar}{2} \left(\vec{\Gamma}_+ \cdot \vec{\lambda}_+ - \vec{\Gamma}_- \cdot \vec{\lambda}_- - \int_{-D}^{D} \vec{\lambda} \cdot \frac{d\vec{\Gamma}}{dt} dt \right)
\end{aligned}
\tag{25}
$$

where we use the notation $\vec{\Gamma}_-$ and $\vec{\Gamma}_+$ to denote $\vec{\Gamma}(-D)$ and $\vec{\Gamma}(D)$, and similarly for $\vec{\lambda}$ we have $\vec{\lambda}(+)$ and $\vec{\lambda}(-)$. This dissipated power to the bath will be maximum when the rate of change of $\vec{\Gamma}$ is the maximum, i.e. non-adiabatic. We model this mathematically using the delta function.

$$
\frac{d\vec{\Gamma}}{dt} = \left(\vec{\Gamma}_+ - \vec{\Gamma}_- \right) \delta(t)
\tag{26}
$$

where $\vec{\Gamma}_+$ and $\vec{\Gamma}_-$ are the values of the Hamiltonian "before" and the "after" the transition. Using this model and the integral property of the delta function, $\int f(t)\delta(t)dt = f(0)$, we have

$$
E_{diss} < \frac{\hbar}{2} \left(\vec{\Gamma}_+ \cdot \vec{\lambda}_+ - \vec{\Gamma}_- \cdot \vec{\lambda}_- - \vec{\lambda}(0) \cdot (\vec{\Gamma}_+ - \vec{\Gamma}_-) \right)
\tag{27}
$$

As mentioned before, we assume that $D \gg \tau$, i.e. the system is in equilibrium with the heat bath at $t = -D$ and $t = D$. In such case, we have $\lambda(0) = \lambda_- = \lambda_-^{ss}$ and $\lambda_+ = \lambda_+^{ss}$. Using these observations, we can show that

$$
E_{diss} < \frac{\hbar}{2} \vec{\Gamma}_+ \cdot \left(\vec{\lambda}_+^{ss} - \vec{\lambda}_-^{ss} \right)
\tag{28}
$$

$$
P = \frac{E_{diss}}{T_c} < \frac{\hbar}{2T_c} \vec{\Gamma}_+ \cdot \left(-\frac{\vec{\Gamma}_+}{|\vec{\Gamma}_+|} \tanh \left(\frac{\hbar|\vec{\Gamma}_+|}{kT} \right) + \frac{\vec{\Gamma}_-}{|\vec{\Gamma}_-|} \tanh \left(\frac{\hbar|\vec{\Gamma}_-|}{kT} \right) \right)
\tag{29}
$$

where we have characterized the power dissipation as the energy per clock cycle; T_c is the clock period. As is evident, the power upper bound can be derived once we have the before and after Hamiltonian for the three power dissipating events. These values of the Hamiltonian are as shown in Table I. The "leakage" power dissipated (energy per clock cycle) is the energy dissipated during the first and the third event associated with clock change. And, the "switching" power (energy per clock cycle) is the energy loss due to the second event.

TABLE I

BLOCH HAMILTONIAN BEFORE AND AFTER A CHANGE IN CLOCK OR THE NEIGHBORING POLARIZATION

		Clock Up $\gamma_L \to \gamma_H$			Driver Polarization $G_- \to G_+$			Clock Down $\gamma_H \to \gamma_L$	
$\vec{\Gamma}_- =$	$\frac{1}{\hbar}\left[\right.$	$-2\gamma_L,$	$0,$	$\left.G_-\right]$ $\frac{1}{\hbar}\left[\right.$	$-2\gamma_H,$	$0,$	$\left.G_-\right]$ $\frac{1}{\hbar}\left[\right.$	$-2\gamma_H,$	$0,$ $\left.G_+\right]$
$\vec{\Gamma}_+ =$	$\frac{1}{\hbar}\left[\right.$	$-2\gamma_H,$	$0,$	$\left.G_-\right]$ $\frac{1}{\hbar}\left[\right.$	$-2\gamma_H,$	$0,$	$\left.G_+\right]$ $\frac{1}{\hbar}\left[\right.$	$-2\gamma_L,$	$0,$ $\left.G_+\right]$

VI. ENERGY DISSIPATED PER CLOCK CYCLE IN A QCA CIRCUIT

Since the physics governing the power dissipation at each cell in a QCA circuit is similar, we can compute the total power (energy per clock cycle) by aggregating the power computed for each cell. The effect of cells on each other is captured through the electrostatic kink energy between them. Let us consider a circuit with N cells, denoted by $X_1, \cdots, X_N$, with the first r of them representing the input cells. Let the polarization of the i-th cell be denoted by $x_i \in [-1, 1]$. For each switching of the input cells, we compute the power by keeping track of the before and after polarization of the cells. Let $x_{i|k}$ be the polarization of the i-th cell for the k-th possible input combination. We can compute this polarization using any of the simulation methods that are available for QCA circuits [27]. In our experiments we use the Bayesian Network modeling technique in [1] to probabilistically determine the polarizations in an efficient manner. Since in this work, we are interested in an upper bound on the total power dissipated in a circuit, we actually round off the computed polarization of each cell to the nearest pure value, i.e. -1 or 1 value. In actual circuits, the polarization will be lower in magnitude than 1. So the estimate we get will be more than the actual power expenditure. For circuits, with large clock zones, the absolute values of the polarization will tend to deviate more from the 1/-1 due to increased possibilities of excited states. For such cases, our estimates will still hold, although they will not be as tight.

To compute the power dissipated at each cell, we need to compute the effective kink energy of rest of the cells, G_{i-} and G_{i+} as the input switches from k-th combination to the m-th combination. This is easily computed as

$$G_{i-} = \sum_{j \in Ne(X_i)} E_k f_j x_{j|k} \text{ and } G_{i+} = \sum_{j \in Ne(X_i)} E_k f_j x_{j|m} \tag{30}$$

where the sum can be restricted to a local neighborhood of the cell since the distance related term, f_j, falls off as 5-th power of the distance from the cell. Using these values, and knowledge of the low and the high clock energies, γ_L and γ_H, we can compute the leakage ($P_{i,k \to m}^{leak}$) and the switching ($P_{i,k \to m}^{switch}$) power (energy per clock cycle) bounds at each cell (Eq. 29). Given these estimates we can compute different design related parameters as outlined below. Note that the quantities we compute are actually bounds of the respective quantities; we do not emphasize the bound aspect to reduce notational clutter. We also note that this time we do not account for variation of clocking energies within a zone that might happen, depending on the choice of the specific technology for clocking. However, such knowledge can be easily incorporated by using a spatially varying clocking energy in the expressions for the

bounds.

1) **Total Dissipated Power:** for transition from the *k*-th input state to the *m*-th input state is given by

$$P^{tot}_{k \to m} = \sum_{i=(r+1)}^{N} P^{leak}_{i,k \to m} + P^{switch}_{i,k \to m} \tag{31}$$

2) **Average Power over all input transitions** is given by

$$P^{avg} = \frac{1}{2^r} \sum_{k,m} P^{tot}_{k \to m} \tag{32}$$

3) **Maximum Power over all input transitions** is given by

$$P^{max} = \max_{k,m} P^{tot}_{k \to m} \tag{33}$$

4) **Hot Spots:** Power is not uniformly dissipated at each cell. It is important from an thermal error analysis point of view to identify the cells in a design where the power dissipation is high. The term hot spots is used for cells that dissipate considerably higher energy as compared to most of the neighboring QCA cells. We have observed that thermal hot spots usually form at QCA cells that are critical to the operation of a QCA circuit, such as the middle cell of a simple majority gate. Once we compute the average power dissipation at each cell over all input transitions, we can identify the hot-spot as the cells with *n* maximum power dissipation.

$$\arg \text{n-max}_{\text{all cells}} \{ \frac{1}{2^r} \sum_{k,m} P_{i,k \to m} | i = r+1, N \} \tag{34}$$

VII. RESULTS

We first present empirical validation of the power bounds by computing exact power of one QCA cell under different clocking conditions and show that the bound holds. We follow this by showing examples of how this bound estimate can be used for QCA design automation. The size of QCA cells used in this study is 20nm x 20nm with a grid spacing of 10nm.We compute power dissipation bounds for some basic QCA logic elements such as the inverter, crossbar and clocked majority gate. Since power is dependent on the inputs, we show the maximum, minimum and average power dissipated in each of these circuits over all possible input transitions. Further, we make use of the model to estimate power dissipated in two different designs of single bit adders and show the thermal layout for both designs. Finally, we demonstrate the model for some large circuits – the 4x1 multiplexer and a single bit ALU design [21]. The ALU design consists of seven inputs and two outputs. The single bit ALU can be used to perform logical operations such a AND, OR and inversion. It can also perform mathematical operations such as addition and subtraction between two single bit numbers. The results in this section are based on the assumptions that the technology to provide clocking to a QCA circuit exists and this model does not take into account the power dissipation due the clocking circuit as well as the distance of a QCA cell from the clocking mechanism.
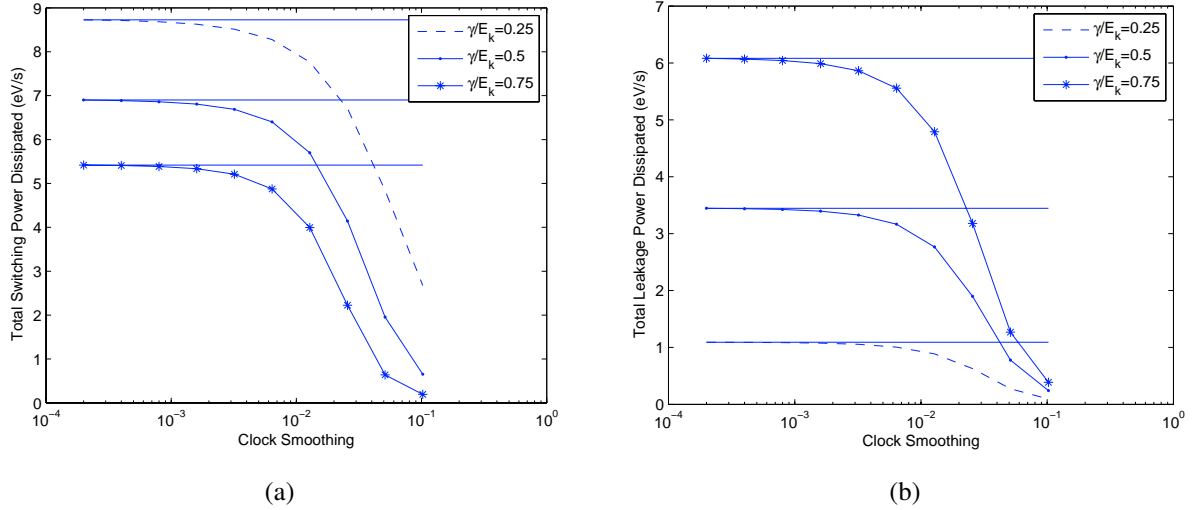
Fig. 3. Variation of (a) switching power and (b) leakage power dissipated in a single cell with different amount of clock smoothing for different clock energy γ levels. Adiabaticity of the switching process is controlled by smoothness of the clock transition. The horizontal line plots the upper bounds for each case as computed using the derived expressions.

A. Energy dissipation per clock cycle in a single QCA cell

The power dissipated at each cell is a function of the rate of change of the clock and the clock energy. We estimated the actual power dissipated using quantum model for various values of these parameter and compared them with the power bounds. Fig. 3(a) and (b) shows the variation of switching and leakage power dissipation with varying amount clock smoothing and for different values of clock energy. The power bounds, which are functions of the clock energy(γ), are shown as horizontal lines. Adiabaticity of the system is directly proportional to the amount of clock smoothing. Higher clock smoothing implies more adiabaticity. We used Gaussian functions to implement smooth clocks. We see that bounds do indeed hold and are reached when the clock smoothing is zero, i.e. abrupt clock changes, representing the fully non-adiabatic case.

Fig. 4 shows how the dissipated energy bound is different for different state transitions (a) 0→0 (b) 0→1 (c) 1→0 and (d) 1→1, as the clock energy supplied to the cell is increased from $0.05E_k$ to $2E_k$. Note that energy is dissipated even if the state of a cell does not change, i.e. for cases (a) and (d). This is because the high clock state only *partially* depolarizes a cell and there is change in this partial polarization with input change. As the high clock energy is increased, the cell gets depolarized to a greater extent and the contribution to overall dissipation due to switching states is less. However, as we see in Fig. 4, the total dissipated energy also increases; this is due to the contribution of dissipative event associated with clock transitions, i.e. "leakage power." So, even though high clock energy is desirable to depolarize the cell and ensure when the clock energy supplied to the cell is increased from $0.05E_k$ to $2E_k$ for correct operation, it has to be limited from power considerations.

For any system that is capacitively coupled to the environment, power dissipation will not be independent of the error. Fig. 5 shows the temperature dependence of power dissipation and polarization error in a QCA cell. We
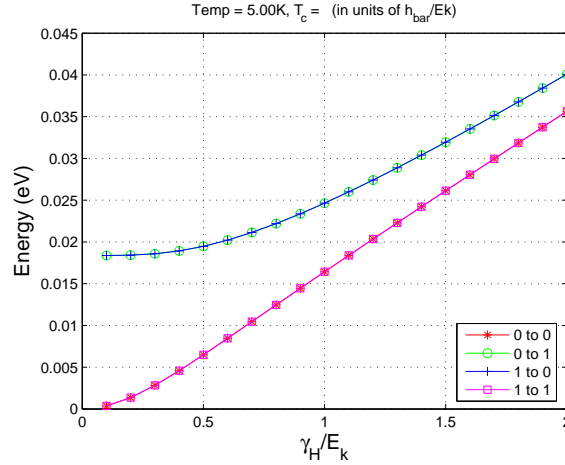
Fig. 4. Dependence of energy dissipated (upper bound) in a cell with clock energy for different clock transitions. (a) 0→0 (b) 0→1 (c) 1→0 and (d) 1→1. Note that the plots for cases (a) and (d) overlap completely and so does the plots for cases (b) and (c).
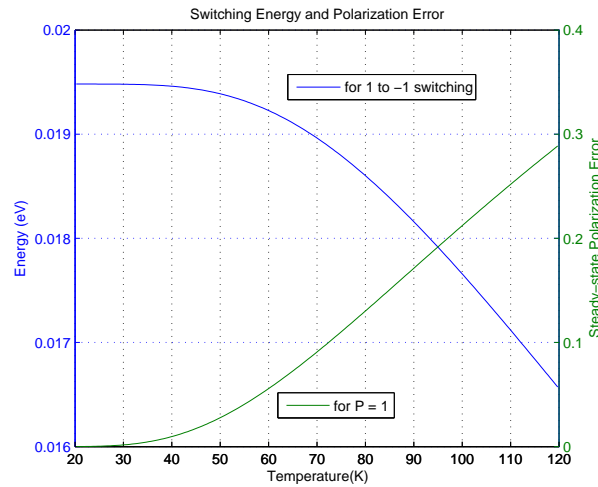

Fig. 5. Variation of power dissipation and steady-state polarization error with temperature. The decrease in polarization energy is almost proportional to the increase in polarization error over higher temperature ranges.

quantified the error based on the computed polarization of the cell. Absolute value of one minus the polarization is the probability of a wrong state at a cell. Similarly, the plot for energy dissipation was obtained from Eqn. 29 by varying the temperature and keeping γ_H constant. It can be seen that as we vary temperature, the polarization error increases, however, the energy dissipation of the cell goes down. Energy dissipation and error are inversely related as the temperature is changed.

B. Energy dissipation per clock cycle in basic QCA circuits

We consider arrangements of QCA cells implementing crucial QCA circuit elements. In Table II for each circuit, we visualize the energy dissipated at each cell, averaged over different input transitions. We use grayscale shading to

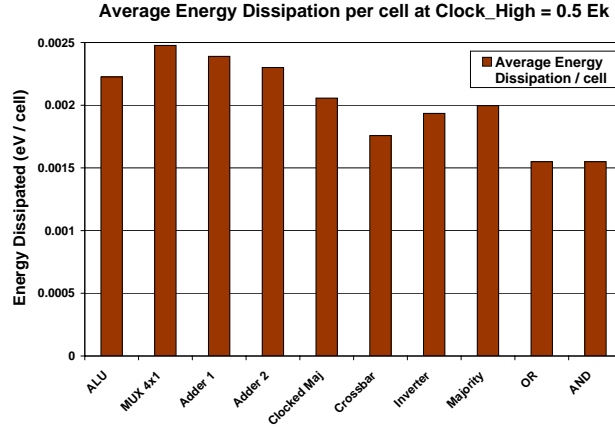**Average Energy Dissipation per cell at Clock_High = 0.5 Ek**

Fig. 6. Energy dissipation bounds per cell for different QCA logic elements, averaged over different input combinations. The number of cells for each circuit refers to the number of cells that dissipate energy during a switching event. The graph shown here is for $\gamma/E_K = 0.5$. Note that the color mapping scale for each circuit is different.

visualize the dissipation at each cell – darker the cell, more the dissipation. We will refer to this kind of visualization as the *thermal layout*. Note that the dissipation scale for each circuit is different. We can clearly see that not all the cells of the circuits dissipate same amount of energy.
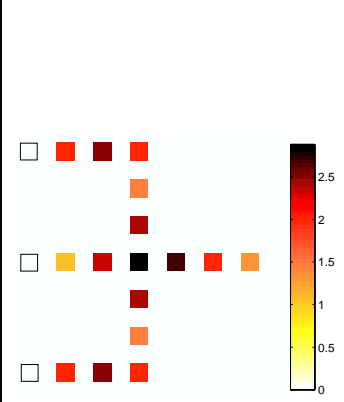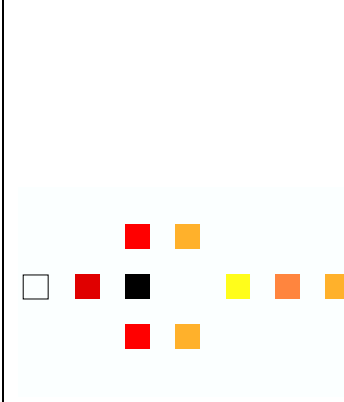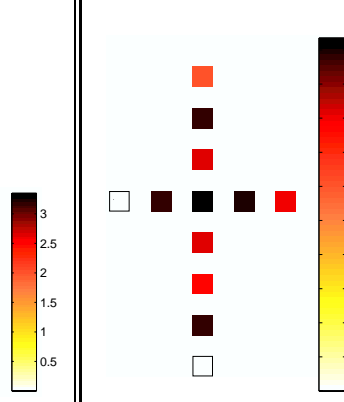
In addition to the energy dissipation, averaged over all input combinations, we also show the maximum dissipation over all input conditions and the minimum dissipation over all input conditions. The minimum energy dissipation case is when the input cells do not switch. These three quantities convey some idea about the overall variability of the dissipation with input. We have tabulated these results for three values of E_k.

The number of cells in the table refer to the number of cells that participate in energy dissipation. We do not include input cells in calculating the total energy dissipation. We can see, that in case of a clocked majority gate shown in Table II(a) even though the total energy dissipated is much higher than that of an inverter shown in Table II(b), weakest spots, i.e. cell with the highest dissipation in its neighborhood, in the inverter design dissipate higher amount of energy than that in a majority logic. This is evident from the scale associated with the color code. If we consider the weakest link in a design to be the determinant of reliability then the inverter is more susceptible to thermal breakdown. However, we should also note that many cells in the majority logic have high dissipation, close to the maximum value.

We can also see that even though the energy dissipated for the circuits listed in Table II greatly depends on the number of cells for each design, still the average (over all input combinations) energy dissipation *per cell* for clocked majority gate, inverter, crossbar and simple majority gate does not vary greatly as can be seen from the graph shown in Fig. 6. This suggests that modeling power dissipation in QCA circuits to scale linearly with the number of cells is a reasonable one, however, this needs to be established on firmer empirical footing using more circuit designs with larger number of cells.

TABLE II

THERMAL LAYOUT OF AVERAGE ENERGY DISSIPATED (OVER DIFFERENT INPUT TRANSITIONS) AT EACH CELL FOR SOME BASIC QCA

LOGIC ELEMENTS. DARKER THE COLOR, MORE THE DISSIPATION.

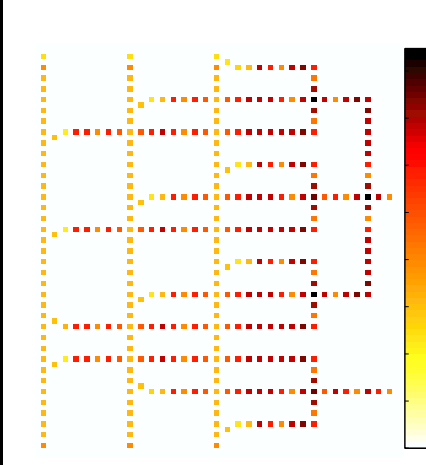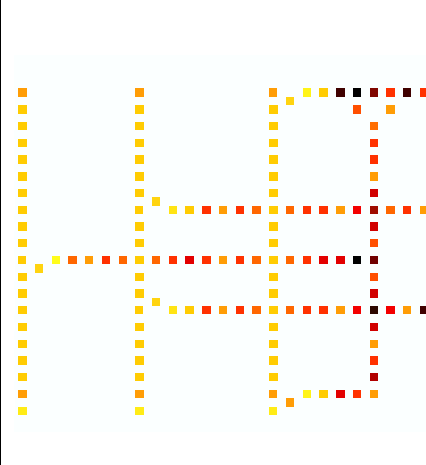|	(a) Clocked Majority			(b) Inverter			(c) Crossbar		
No. of Cells	16			9			10		
Thermal Layout at γ/E_K=0.5 (Energy Dissipation scale is in terms of 10^{-3} eV)									
γ/E_K	0.5	1.0	1.5	0.5	1.0	1.5	0.5	1.0	1.5
Avg E_{diss}(meV)	32.91	39.10	47.48	17.41	21.26	26.16	17.58	26.01	35.70
Max E_{diss}(meV)	71.99	73.84	77.76	31.76	33.54	36.58	28.52	33.67	41.36
Min E_{diss}(meV)	4.27	13.86	25.49	3.06	8.97	15.75	6.97	18.37	29.98

C. Energy dissipation per clock cycle in QCA Adder circuits

Table III shows the comparative study of energy dissipated in two different QCA adders designs. As we can see from the table, Adder-1 has much higher energy dissipation, as it has 359 energy dissipating QCA cells present in its layout as compared to Adder-2 design that has only 165 such cells. We can see from the table that thermal energy layout for each design shows that the highest average energy dissipation for any particular cell in both designs is almost the same, even though the Adder-2 design has comparatively larger number of such 'high energy dissipation' dissipating cells present in its layout. We can also see from the graph in Fig. 6 that even though the total energy dissipation for both designs may vary greatly, still the average (over all input) power dissipation *per cell* is almost the same for both designs. For both designs, the maximum energy dissipation occurred when the input combinations switched from 000→111.

This result seem to be interesting because it has been already shown in [10] that Adder-2 design is more prone to error than Adder-1 design. Whereas, we can see that when it comes to power, Adder-2 is more energy efficient even though it has more hot-spots present in its layout.

TABLE III

THERMAL LAYOUT OF AVERAGE ENERGY DISSIPATED (OVER DIFFERENT INPUT TRANSITIONS) AT EACH CELL FOR TWO QCA ADDER DESIGNS.

	(a) Adder 1			(b) Adder 2		
No. of Cells	359			165		
Thermal Layout at γ/E_K=0.5 (Energy Dissipation scale is in terms of 10^{-3} eV)						
γ/E_K	0.5	1.0	1.5	0.5	1.0	1.5
Avg E_{diss} (meV)	857.74	1110.45	1421.66	379.56	499.44	645.18
Max E_{diss} (meV)	1524.42	1655.32	1868.33	671.80	736.98	840.29
Min E_{diss} (meV)	203.82	576.53	984.33	97.42	271.06	458.34

D. Energy Dissipation per clock cycle in large QCA circuits

In order to demonstrate that this work is applicable to even larger designs, we also present the results for a 4x1 multiplexer and a single bit ALU designs. The ALU design consists of over 800 QCA cells. Fig. 7 shows the thermal layout for average power dissipated at each cell in a 4x1 multiplexer design. We can clearly see the thermal hot-spots in the design. We see that the branching at the middle of the design and the inverter in the design have the weakest spots in the design. These hot spots dissipate large power, averaged over all input combinations, and in order to make the designs less susceptible to thermal breakdowns, designers can target these weak spots in the design for further reinforcements. The fabrication scientists can also use these results to select different types of devices.

Apart from calculating the thermal layout for the average energy dissipation in an ALU design, we also studied the thermal energy layout in case of maximum and minimum energy, over all input transitions. In Fig. 8(a) and(b) we show the thermal layout of ALU circuit for the maximum and minimum energy dissipation cases, respectively.
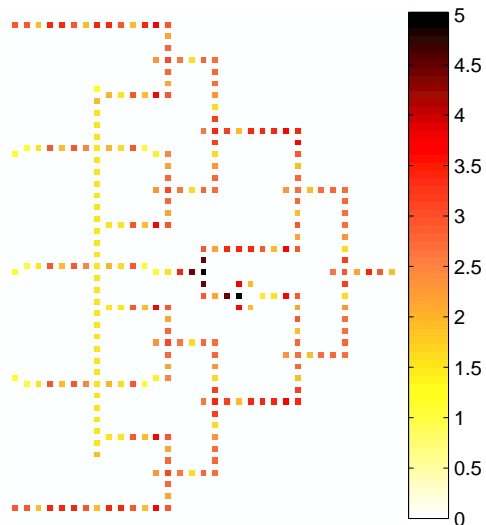
Fig. 7. Thermal Layout for average energy dissipated in each cell of a 4x1 MUX circuit. The dark spots are the ones that dissipate larger amount of energy on an average. The layout was obtained by simulating over all possible input switching combinations from $000000 \rightarrow 111111$ for $\gamma/E_K = 0.5$. The energy dissipation scale for each cell is in terms of 10^{-3} eV.

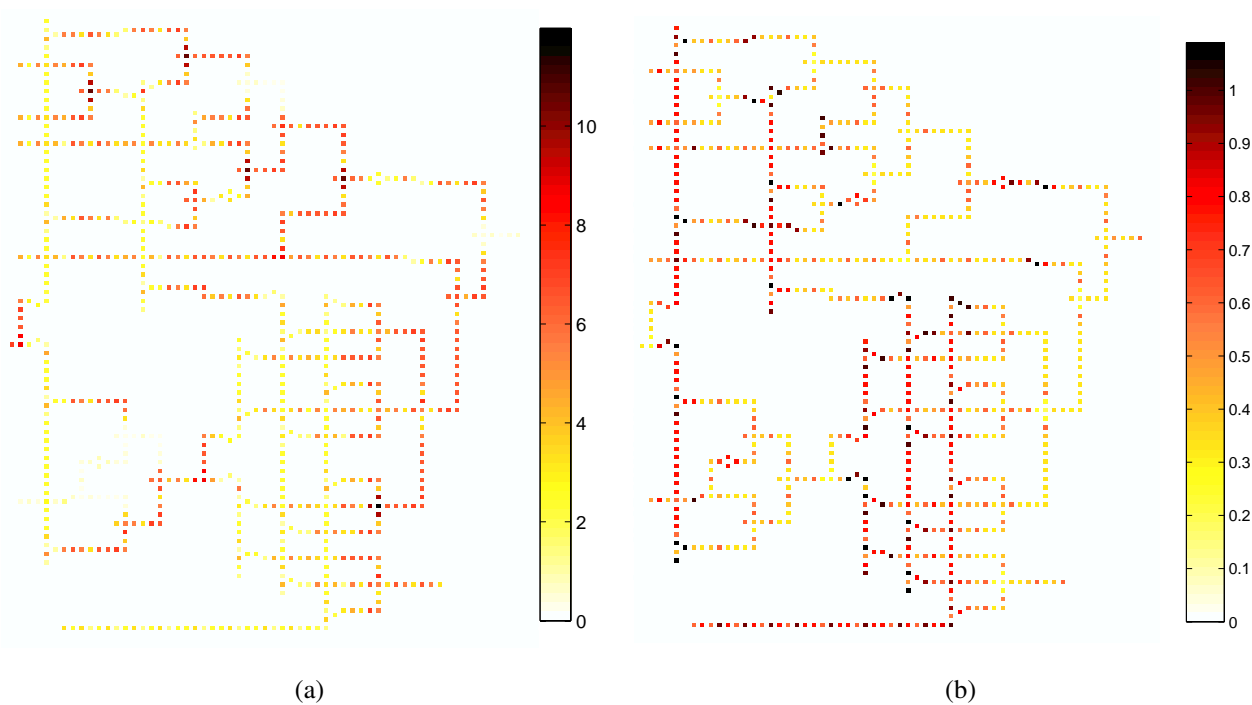(a)   (b)

Fig. 8. Thermal Layout for energy dissipated in each cell of an ALU circuit for (a) Maximum energy dissipating input combination and (b) for least energy dissipating input combination. Note that the color code scales are different for these two figures. Energy dissipation scale is in multiples of 10^{-3}. The dark spots are the ones that dissipate larger amount of energy. The layout was obtained by simulating worst case and best case input switching vectors at $\gamma/E_K = 0.5$. The energy dissipation scale in (b) is much smaller than that in (a) since energy is dissipated only due to leakage component and hence is much less than (a) where switching energy plays a dominant role in total energy dissipation of a cell.
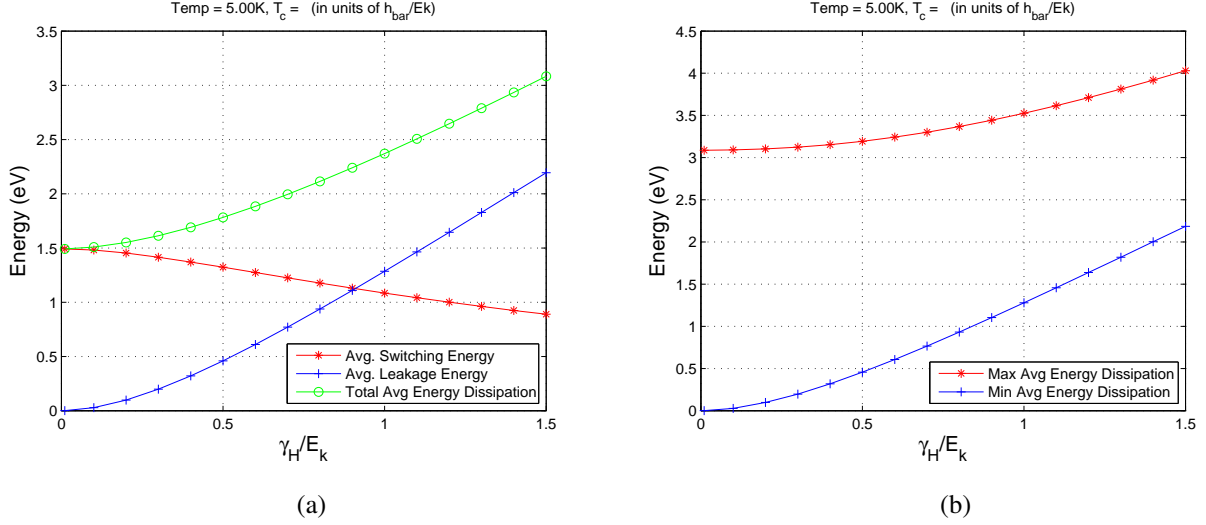
Fig. 9. Graphs showing energy dissipated in a QCA ALU circuit (a) Shows the variation of leakage and switching components of energy dissipated for various values of γ/E_K (b) Shows the variation in maximum and minimum energy dissipated for various values of γ/E_K

Note that the color code scales are different for these two designs. It can be clearly seen from the layouts that the energy dissipated in almost all cells of Fig. 8(a) is more than that of cell dissipating highest energy in Fig. 8(b). On an average each cell in Fig. 8(a) dissipates a magnitude higher energy than that in case of Fig. 8(b). The reason behind this is that in case of minimum power dissipation, none of the input cells switch state. And the total energy dissipated at each cell in this case is only the leakage energy (which is quite low compared to the switching component of energy). However, this conclusion is not valid for higher clock energies.

In Fig. 9(a) we plot the variation of the dissipation (averaged over all input transitions) with clock energy. We see that switching component of energy reduces when we increase the clock energy, but the leakage component increases much more significantly, resulting in overall increase in power dissipation. At $\gamma \approx 0.9 E_K$, the leakage component of energy and switching component contribute equally to the total energy dissipation of the circuit. Beyond this value of γ, the leakage component of energy dissipation contributes more than the switching component towards total energy dissipation. Fig. 9(b) shows the variation of maximum and minimum energy dissipation in a QCA ALU design with respect to the clock energy. We can see that while it is desirable to have higher clock energy in order to reduce errors in QCA operation [14], it can be seen clearly from the results that if the clock energy is raised significantly, the energy dissipation is high.

VIII. CONCLUSION

We used a quantum mechanical power model coupled to a dissipative environment to derive the upper bound for power dissipation in QCA cells. These bounds were then used to estimate power bounds for each cell in QCA circuits. Power dissipation in QCA increases with clock non-adiabaticity and the upper bound corresponds to the case when the clock is square shaped. We also established correspondence with the concepts of "leakage" and

"switching" power in CMOS circuits. These theoretical bounds were then used to compute power at each cell in QCA circuits. In this paper we have not considered the tradeoffs between error and power. There is extensive discussions in the literature [28], [29], [30] about the general relationships between power dissipation and error tolerance. Although in principle very low power dissipation is possible, attention needs to be paid towards error tolerance. As per the guidelines laid down for emerging research devices in [31], thermal fluctuations will require energy barriers of order $Nk_BTln(2)$ for reliable computing (where $N > 10$). In this work, we found the value of N to be greater than 50, with the N for the maximum power dissipating QCA cell in the ALU circuit as 103. Of course, ours is an upper bound estimate and not inconsistent with the lower estimates obtained with fully adiabatic clocks. More detailed analysis of the tradeoff between error tolerance and power, in the presence of defects, is a topic of future research.

This power model can be extended for molecular and magnetic QCAs by using the appropriate Hamiltonian in the derivation. The Hamiltonian for molecular QCA has already been presented by Lent *et. al.* in [4]. The exact power equations will change, but the basic structure of the derivation will remain the same. For the magnetic QCAs, there has been work by Csaba *et. al.*[32] that presents the Landau-Lifshitz equation in Bloch form for a two state magnetic system. However in case of magnetic QCAs, the theory will need to be altered to estimate the steady state polarization values.

The main contribution of this work is that we can compute quickly the worst case power dissipated at each individual cell in a circuit for any input vector transition. The alternative method for estimating power is through coherence vector simulation, which will result in better estimates, but it is time consuming. We need just the estimates of states, before and after an input change. These states can be estimated using a variety of fast methods. We used the probabilistic method in [1], which is more than two orders of magnitude faster than coherence vector approach. With this model, we can locate cells in a circuit, early on in the design process, that are critical in terms of power dissipation and also identify the input vector transitions that result in large power dissipations. We also showed the effect of clock energy on the overall power dissipated in a QCA circuit. We demonstrated this power model using basic QCA circuits like majority gate, inverter, AND gate, OR gate, crossbar and clocked majority gate. We used it to conduct power studies of larger circuits too, such as single bit adders, 4x1 multiplexer and for a single bit ALU. The power model proposed in this work, along with methods for defect analysis [11], [12] and error analysis [9], [10], will be useful to circuit designers and fabrication scientists in providing a more complete picture of the QCA operations.

REFERENCES

[1] S. Bhanja and S. Sarkar, "Probabilistic Modeling of QCA Circuits Using Bayesian Networks," *IEEE Transactions on Nanotechnology*, vol. 5, pp. 657–670, Nov. 2006.

[2] A. Orlov, R. Kummamuru, R. Ramasubramaniam, C. Lent, G. Bernstein, and G. Snider, "Clocked quantum-dot cellular automata shift register," *Surface Science*, vol. 532, pp. 1193–1198, 2003.

[3] C. Lent, B. Isaksen, and M. Lieberman, "Molecular quantum-dot cellular automata," *Journal of American Chemical Society*, vol. 125, pp. 1056–1063, 2003.

[4] Y. Lu, M. Liu, and C. Lent, "Molecular quantum-dot cellular automata: From molecular structure to circuit dynamics," *Journal of Applied Physics*, vol. 102, no. 3, p. 034311, 2007.

[5] J. Jiao, G. Long, L. Rebbouh, F. Grandjean, A. Beatty, and T. Fehlner, "Properties of a Mixed-Valence (Fe II)2(Fe III)2 Square Cell for Utilization in the Quantum Cellular Automata Paradigm for Molecular Electronics," *Journal of the American Chemical Society*, vol. 127, no. 50, pp. 17819–17831, 2005.

[6] G. Bernstein, "Quantum-dot cellular automata by electric and magnetic field coupling," *Custom Integrated Circuits Conference*, pp. 223–229, Sept 2003.

[7] A. Imre, G. Csaba, L. Ji, A. Orlov, G. H. Bernstein, and W. Porod, "Majority Logic Gate for Magnetic Quantum-Dot Cellular Automata," *Science*, vol. 311, no. 5758, pp. 205–208, 2006.

[8] S. Bhanja and S. Sarkar, "Themal Switchig Error Versus Delay Tradeoffs in Clocked QCA Circuits," *IEEE Transactions on Very Large Scale Integration(VLSI) Systems*, vol. 16, pp. 528–541, May 2008.

[9] S. Bhanja, M. Ottavi, F. Lombardi, and S. Pontarelli, "Novel designs for thermally robust coplanar crossing in QCA," *Design Automation and Test in Europe*, vol. 1, March 2006.

[10] S. Srivastava and S. Bhanja, "Hierarchical Probabilistic Macromodeling for QCA Circuits," *IEEE Transactions on Computers*, vol. 56, pp. 174–190, Feb 2007.

[11] M. Tahoori, J. Huang, and F. Momemjadeh, M. Lombardi, "Testing of Quantum Cellular Automata," *IEEE Transactions on Nanotechnology*, vol. 3, no. 4, pp. 432–442, 2004.

[12] T. Dysart and P. Kogge, "Strategy and prototype tool for doing fault modeling in a nano-technology," in *IEEE Nano Conference*, vol. 2, pp. 356–359, August 2003.

[13] M. Momenzadeh, J. Huang, M. Tahoori, and F. Lombardi, "Characterization, Test and Logic Synthesis of And-Or-Inverter Gate Design for QCA Implementation," *IEEE Transactions on Computer-Aided Design of Integrated Circuits and Systems*, vol. 24, pp. 1881–1893, Dec 2005.

[14] J. Timler and C. Lent, "Power gain and dissipation in quantum-dot cellular automata," *Journal of Applied Physics*, vol. 91, pp. 823–831, January 2002.

[15] J. Timler and C. Lent, "Maxwell's demon and Quantum-dot Cellular Automata," *Journal of Applied Physics*, vol. 94, pp. 1050–1060, July 2003.

[16] M. Liu and C. Lent, "Power dissipation in clocked quantum-dot cellular automata circuits," *Device Research Conference*, vol. 1, pp. 123–124, June 2005.

[17] M. Lent, C.and Liu and Y. Lu, "Bennett clocking of Quantum-dot cellular Automata and Limits to binary logic scaling," *IEEE Transactions on Nanotechnology*, vol. 17, pp. 4240–4251, August 2006.

[18] J. Huang, M. Xiaojun, and F. Lombardi, "Energy Analysis of QCA Circuits for Reversible Computing," *IEEE Conference on Nanotechnology*, vol. 1, pp. 39–42, June 2006.

[19] L. Bonci and M. Macucci, "Analysis of Power Dissipation in clocke Quantum Cellular Automaton Circuits," *Solid State Device Research Conference ESSDERC*, pp. 57–60, Sept 2006.

[20] S. Srivastava, S. Sarkar, and S. Bhanja, "Power Dissipation Bounds and Models for Quantum-dot Cellular Automata Circuits," *IEEE Conference on Nanotechnology*, vol. 1, pp. 375–378, June 2006.

[21] M. Niemier and P. M. Kogge, "Exploring and exploiting wire-level pipelining in emerging technologies," in *Proceedings of the 28th annual International Symposium on Computer Architecture*, pp. 166 – 177, 2001.

[22] D. P. Tougaw and C. S. Lent, "Dynamic behavior of Quantum Cellular Automata," *Journal of Applied Physics*, vol. 80, pp. 4722–4736, Oct 1996.

[23] G. Mahler and V. A. Weberruss, *Quantum Networks: Dynamics of Open Nanostructures*. Springer Verlag, 1998.

[24] U. Weiss, *Quantum Dissipative Systems*. World Scientific Publishers, 1998.

[25] M. Menskii, "Dissipation and decoherence in quantum systems," *Physics-Uspekhi*, vol. 46, no. 11, pp. 1163–1182, 2003.

[26] G. Lindblad, "On the generators of quantum dynamical semigroups," *Communicationsin Mathematical Physics*, vol. 48, pp. 119–130, June 1976.

[27] K. Walus, T. Dysart, G. Jullien, and R. Budiman, "QCADesigner: A Rapid Design and Simulation Tool for Quantum-Dot Cellular Automata," *IEEE Transactions on Nanotechnology*, vol. 3, pp. 26–29, March 2004.

[28] R. K. Cavin, V. Zhirnov, J. Hutchby, and G. Bourianoff, "Energy barriers, demons, and minimum energy operation of electronic devices (plenary paper)," *Noise in Devices and Circuits III*, vol. 5844, no. 1, pp. 1–9, 2005.

[29] B. K. Laszlo, "End of moore's law: thermal (noise) death of integration in micro and nano electronics," *Physics Letters A*, vol. 305, pp. 144–149, 2002.

[30] S. Bandyopadhyay, "Power dissipation in spintronic devices: A general perspective," *Journal of Nanoscience and Nanotechnology*, vol. 7, pp. 168–180, January 2007.

[31] "International technology roadmap for semiconductors," in *"http://www.itrs.net/Links/2005ITRS/Home2005.htm"*, 2005.

[32] G. Csaba, *Computing with field-coupled nanomagnets*. PhD thesis, University of Notre Dame, 2004.